Supporting information

Reactivity at the electrode-electrolyte interfaces in Li-ion and gel electrolyte lithium batteries for $LiNi_{0.6}Mn_{0.2}Co_{0.2}O_2$ with different particle sizes

Adrien Soloy[1], Delphine Flahaut[2,4,], Dominique Foix[2,4], Joachim Allouche[2,4], Germain Salvato Vallverdu[2,4], Erwan Dumont[3], Lucille Gal[3], François Weill[1,4,5] and Laurence Croguennec[1,4,5,*]*

[1] Univ. Bordeaux, CNRS, Bordeaux INP, ICMCB UMR 5026, F-33600 Pessac, France

[2] Université de Pau et des Pays de l'Adour, E2S UPPA, CNRS, IPREM UMR 5254, 64000 Pau, France

[3] SAFT, Direction de la Recherche, 33074 Bordeaux, France

[4] RS2E, Réseau Français sur le Stockage Electrochimique de l'Energie, FR CNRS 3459, F-80039 Amiens Cedex 1, France

[5] ALISTORE-ERI European Research Institute, FR CNRS 3104, F-80039 Amiens Cedex 1, France

Table S1. Chemical analyses of the synthesized samples performed by ICP-OES. The Ni:Mn:Co stoichiometry and Li/TM ratio are in good agreement with the expected ones, i.e. Ni:Mn:Co = 6:2:2 and Li/TM ≥ 1.

	ICP-OES			
	Ni/ΣxTM	**Mn/ΣxTM**	**Co/ΣxTM**	**Li/ΣxTM**
930-5-O_2	0.60(3)	0.20(1)	0.20(1)	1.07(8)
900-5-O_2	0.60(3)	0.20(1)	0.20(1)	1.06(7)
810-5-O_2	0.60(3)	0.20(1)	0.20(1)	1.06(7)

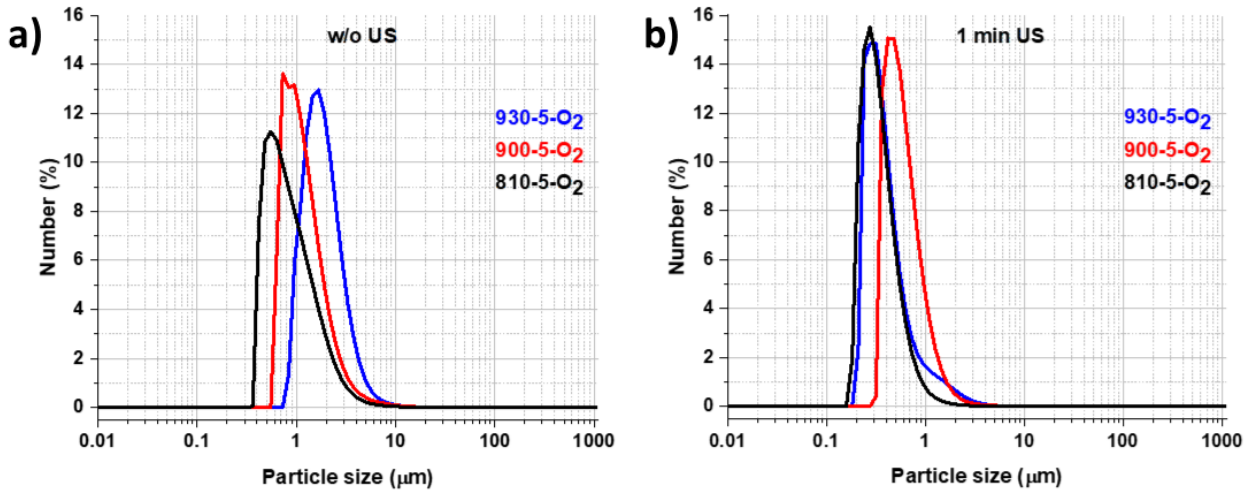

Figure S1. Size distributions obtained by laser granulometry measurements. Results displayed in number percentage without sonication (a) and with 1 min sonication (b). The average primary particle sizes determined here are in good agreement with those obtained after SEM pictures analysis. Larger secondary particles are obtained with larger primary particles.

Table S2. BET surface areas and pore volumes determined for the three samples. The surface area and pore volume decrease slightly because of the increase of primary particle size with the lithiation temperature.

Sample	Average primary particle size	BET surface area (m^2/g)	Pore volume (cm^3/g)
930-5-O_2	2.1 μm	1	0.002
900-5-O_2	810 nm	2	0.003
810-5-O_2	240 nm	3	0.009

Table S3. XPS quantitative analyses of the 810-5-O_2 sample (240 nm particles).

Peak	Assignment	BE (eV)	At. %
C 1s	**C-C/C-H**	285.0	13.6
	C-O	286.5	1.2
	C=O/O-C=O	288.7	1.6
	CO_3	290.0	6.2
Li 1s	**NMC**	54.2	18.3
	Li_2CO_3	55.6	13.0
O 1s	**NMC**	529.2	10.1
	CO_3^{2-}, O-C=O, O=C	531.7	26.8
	O-C	534.6	0.4
Ni 3p	**Ni**	68.1	5.8
Co 3p	**Co**	61.2	1.5
Mn 3p	**Mn**	49.9	1.6

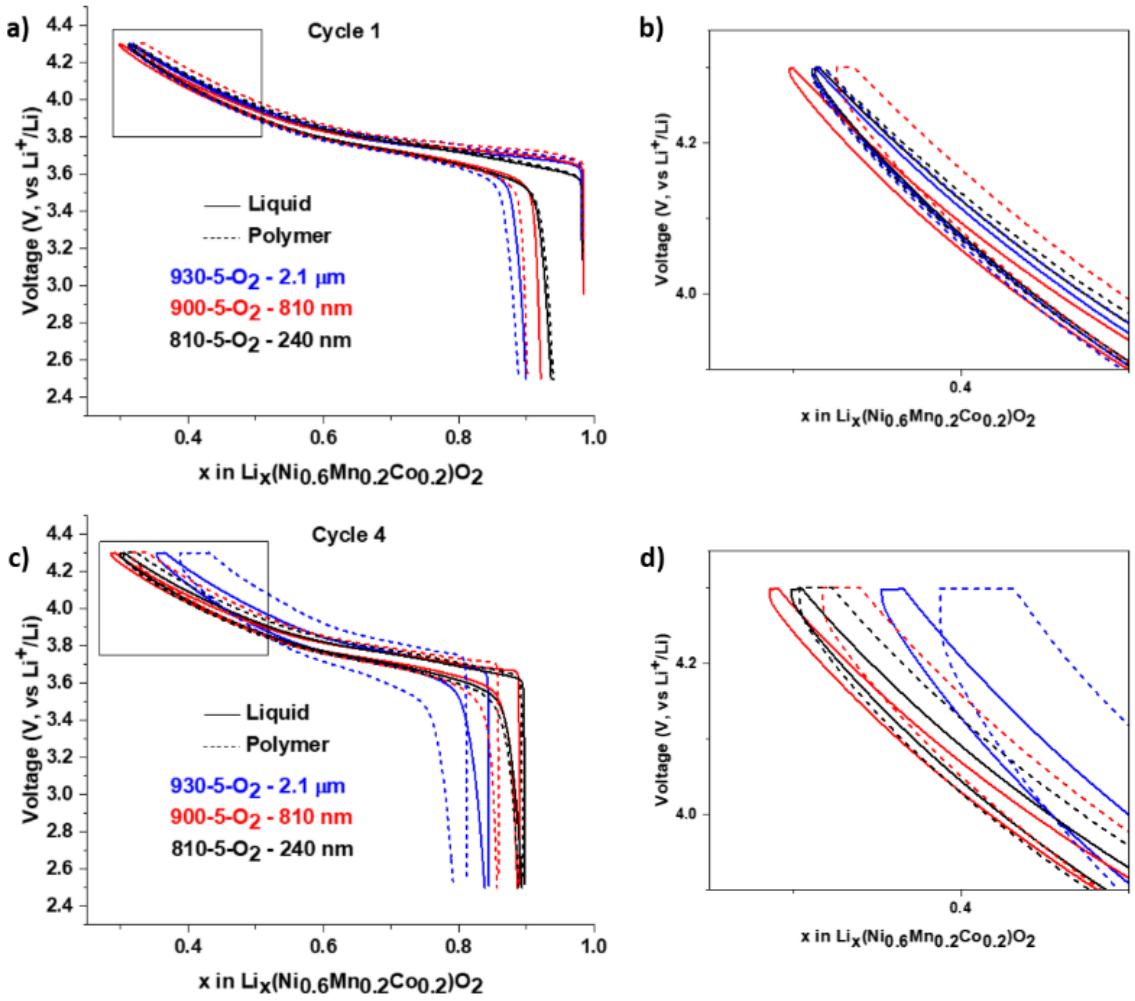

Figure S2. Cycling curves obtained for the three samples in an organic liquid electrolyte and in a gelified electrolyte: 1st cycle (a, b) and 4th cycle (c, d). The samples were cycled at C/5 in the potential window of 2.5-4.3V vs Li^+/Li, after three formation cycles at C/20, C/10 and C/5. The potential is maintained at 4.3V (constant voltage step) until the current becomes smaller than that corresponding to C/85, at the end of every charge. The performances delivered by the 240 nm particles are identical in both types of electrolytes, while those of the 2.1 µm particles decrease rapidly in gelified electrolyte with a significant polarization increase.

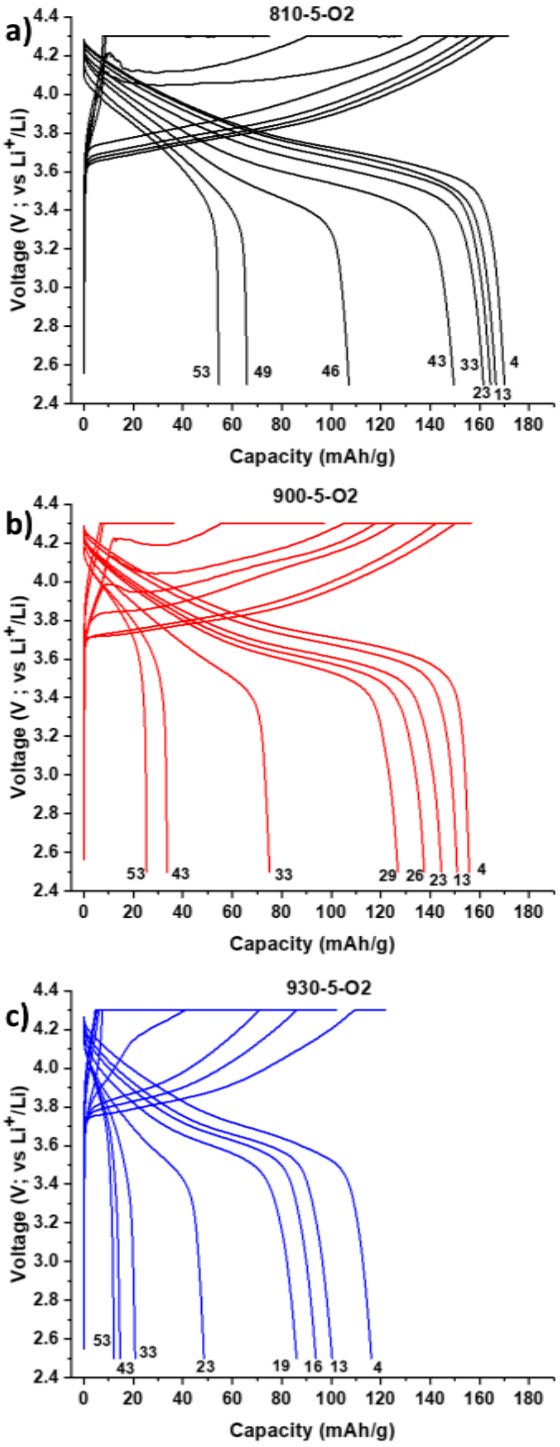

Figure S3. Evolution of the charge-discharge curves for the 810-5-O_2 (240 nm particles) (a), 900-5-O_2 (810 nm particles) (b) and 930-5-O_2 (2.1 µm particles) (c) samples cycled in the gelified electrolyte versus Li metal, at least for cycles 4, 13, 23, 33, 43 and 53, illustrating the capacity drop and polarization increase.

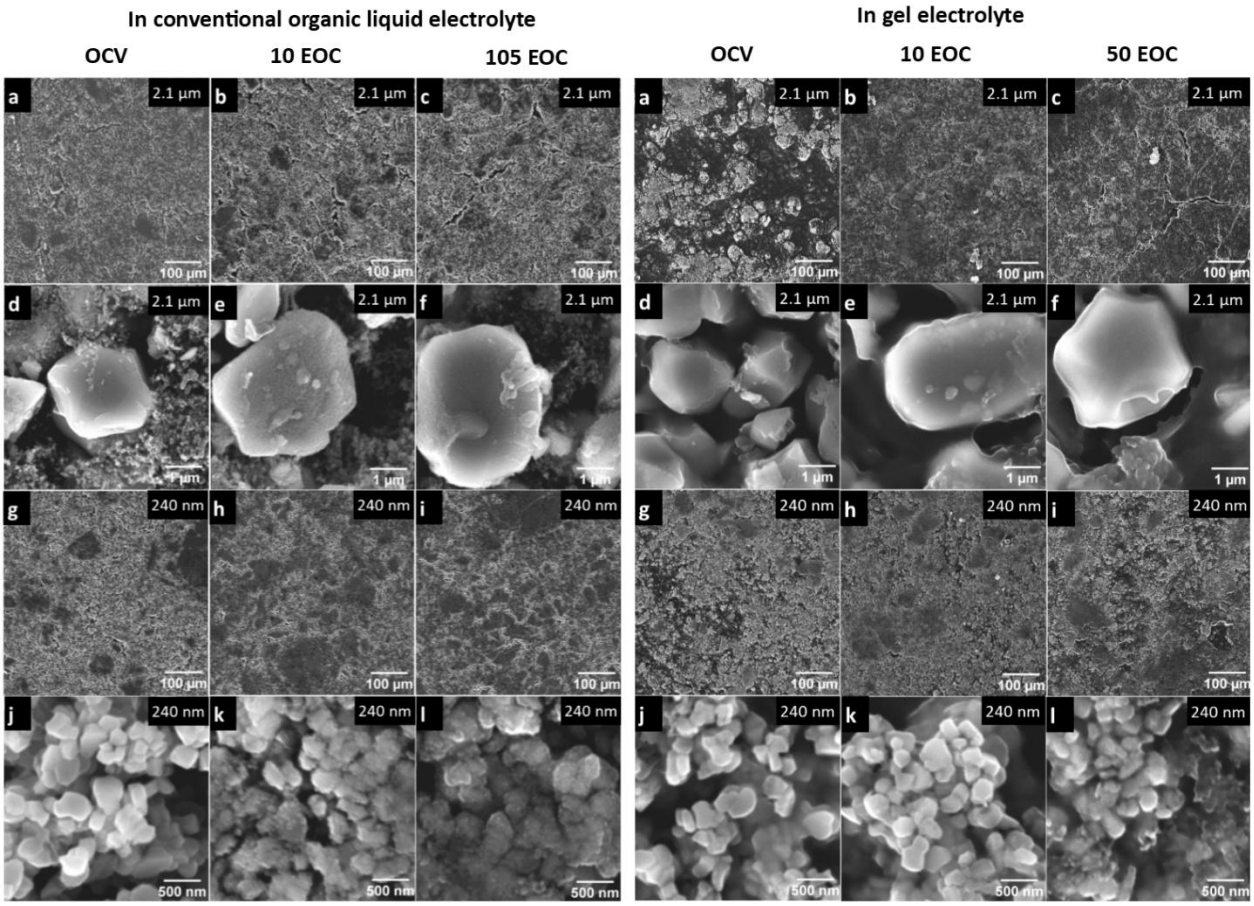

Figure S4. Electrodes morphology observed by SEM after being exposed to the electrolyte (conventional organic liquid electrolyte on the left and gelified electrolyte on the right): in the pristine state without cycling (OCV) (a, d, g, j), after 10 cycles at the end of charge (EOC) (b, e, h, k) and after 105 (or 50) cycles at the end of charge (EOC) (c, f, i, l). SEM images observed for 2.1 µm size particles (a-f) and for 240 nm size particles (g-l) are compared.

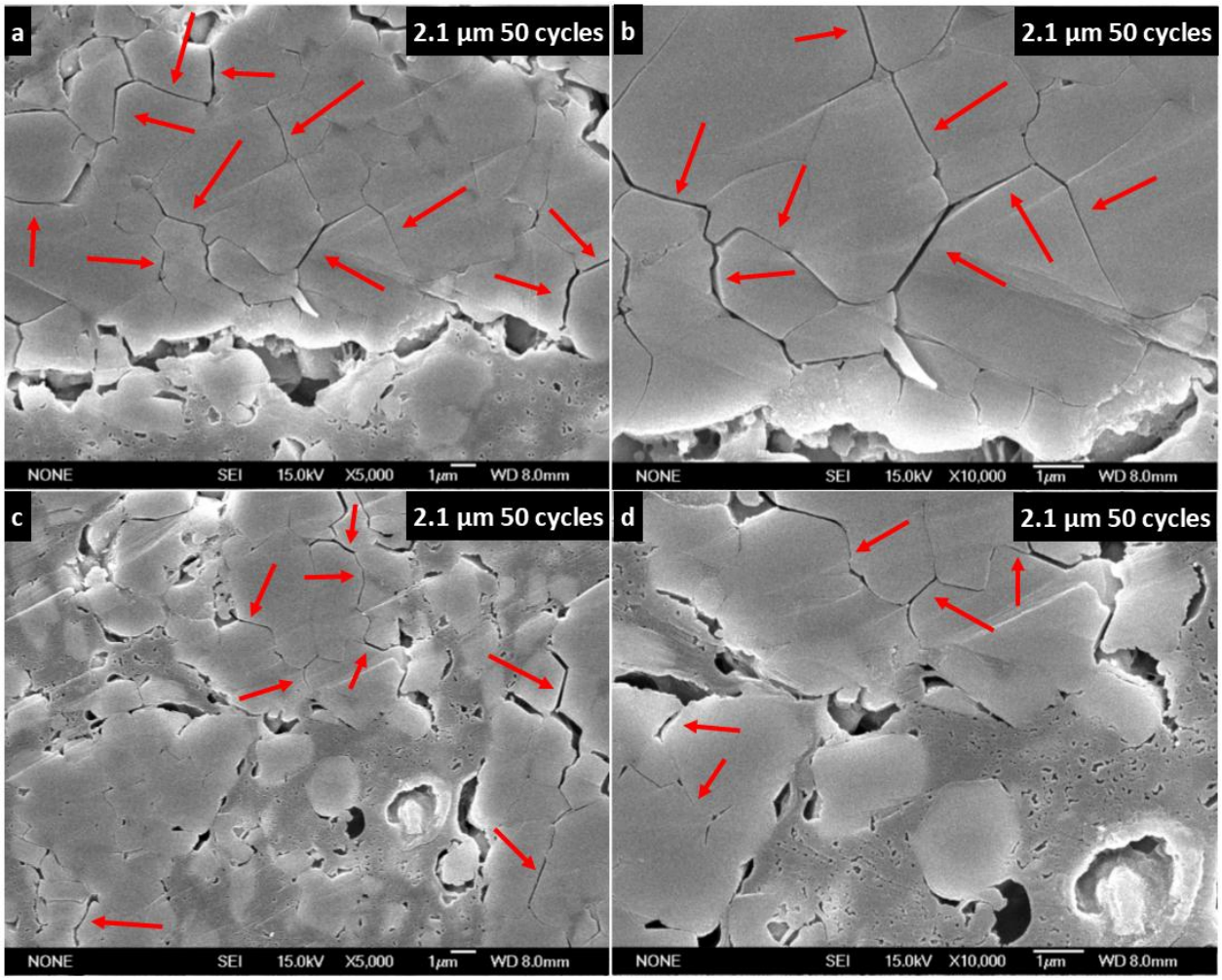

Figure S5. Cross sections of electrodes made of 2.1 µm size particles and observed by SEM after 50 cycles at the end of charge (EOC) in the gelified electrolyte. b and d are magnifications of a and c respectively. In the intergranular spaces highlighted by the red arrows in the aggregates of large particles, it appears that the penetration of the gel was not achieved. Reasonably, it could be one of the origins of the lower performance of the 930-5-O_2 sample (2.1 mm size particles) in all these solid-state batteries.

Table S4. XPS quantitative analyses of the 810-5-O_2 electrode (240 nm particles) after 10 cycles at the end of the charge in the conventional organic liquid electrolyte.

Peak	Attribution	BE (eV)	At. %
C 1s	**C-C/C-H**	285.1	6.9
	C-O	286.3	3.8
	C=O	287.7	4.5
	CO_2	289.0	1.9
	CO_3	290.3	0.8
	CH_2 (PVDF)	286.5	3.1
	CF_2 (PVDF)	291.0	3.1
	CB	284.7	12.8
F 1s	**LiF**	685.1	11.9
	$Li_xPF_yO_z$	686.0	2.1
	CF_2 (PVDF)	688.0	6.5
Li 1s	**NMC**	54.5	2.2
	Li_2CO_3	55.5	2.5
	LiF/$Li_xPF_yO_z$	56.1	24.3
O 1s	**NMC**	529.7	0.3
	CO_3, CO_2, O=C	532.0	2.5
	O-C	532.9	5.0
	O-P	534.5	3.8
Ni 3p	**Ni**	68.0	0.3
Mn 3p	**Mn**	50.0	0.3
Co 3p	**Co**	61.0	0.1
P $2p_{3/2-1/2}$	**$Li_xPF_yO_z$**	135.0	1.5

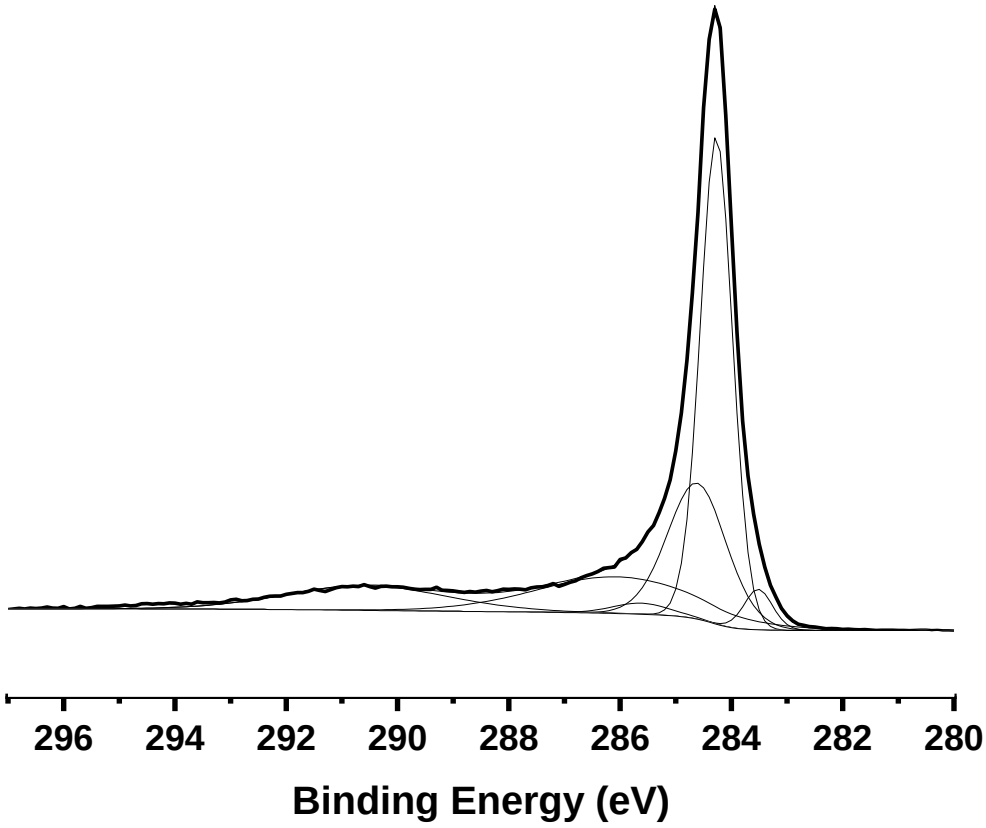

Figure S6. XPS signature of the carbon black used in our electrodes formulation

Table S5. Comparison of the contributions in atomic percentages of carbon black (CB), $LiF/Li_xPF_yO_z$ species and carbonaceous species extracted from the global quantitative analyses performed from XPS spectra of the 810-5-O_2, 900-5-O_2 and 930-5-O_2 electrodes cycled in the conventional organic liquid electrolyte during 10 and 105 cycles and recovered at the end of charge and discharge (referenced as "10 EOC liq", "10 EOD liq", "105 EOC liq" and "105 EOD liq" respectively). They are compared to the contributions obtained for the pristine and OCV electrodes (exposed to the electrolyte without cycling for that latter).

		Pristine electrode	**OCV liq**	**10 EOC liq**	**10 EOD liq**	**105 EOC liq**	**105 EOD liq**
Carbon black (CB)	**930-5-O_2 (2.1 µm)**	38.5	35.2	20.8	22.3	8.1	8.1
	900-5-O_2 (810 nm)	38.9	36.3	26.7	23.4	7.9	9.6
	810-5-O_2 (240 nm)	34.5	30.4	12.8	18.5	1.6	4.2
$LiF/Li_xPF_yO_z$	**930-5-O_2 (2.1 µm)**	2.6	16.2	28.6	26.8	42.6	39.1
	900-5-O_2 (810 nm)	2.9	11.3	17.7	32.5	45.4	44.2
	810-5-O_2 (240 nm)	2.3	13.2	43.6	26.7	64.6	67.7
Carbonaceous species	**930-5-O_2 (2.1 µm)**	23.3	20.1	28.2	26.4	40.4	43.7
	900-5-O_2 (810 nm)	23.3	21.0	27.1	26.6	38.0	39.0
	810-5-O_2 (240 nm)	25.3	18.6	27.9	27.4	25.7	22.6

Table S6. XPS quantitative analyses of the 810-5-O_2 electrode (240 nm particles) after 10 cycles at the end of the charge in the gelified electrolyte (10 EOC gel).

Peak	Attribution	BE (eV)	At. %
C 1s	**C-C/C-H**	285.1	12.4
	C-O	286.5	34.5
	C=O	288.0	1.3
	CO_2	289.1	3.6
	CO_3	290.0	0.4
	CH_2 (PVDF)	286.4	0.6
	CF_2 (PVDF)	290.9	0.6
	CB	284.5	4.5
F 1s	**LiF**	684.7	0.2
	$Li_xPF_yO_z$	686.5	10.0
	CF_2 (PVDF)	688.1	1.1
Li 1s	**NMC**	54.4	0.8
	Li_2CO_3	55.4	0.9
	LiF/$Li_xPF_yO_z$	56.4	3.0
O 1s	**NMC**	529.8	0.5
	CO_3, CO_2, O=C	531.8	1.5
	O-C	532.9	17.5
	O-P	534.0	2.9
Ni 3p	**Ni**	68.0	0.3
Mn 3p	**Mn**	50.0	0.3
Co 3p	**Co**	61.0	0.1
P $2p_{3/2-1/2}$	**$Li_xPF_yO_z$**	135.0	2.7
S $2p_{3/2-1/2}$	**S**	165.0	0.3

Table S7. Comparison of the contributions in atomic percentages of carbon black (CB), $LiF/Li_xPF_yO_z$ species and carbonaceous species extracted from the global quantitative analyses performed from XPS spectra of the 810-5-O_2, 900-5-O_2 and 930-5-O_2 electrodes cycled in the gelified electrolyte for 10 and 50 cycles and recovered at the end of charge and discharge (referenced as "10 EOC sol", "10 EOD sol", "50 EOC sol" and "50 EOD sol" respectively). They are compared to the contributions obtained for the pristine and OCV electrodes (exposed to the electrolyte without cycling for that latter).

		Pristine electrode	**OCV gel**	**10 EOC gel**	**10 EOD gel**	**50 EOC gel**	**50 EOD gel**
Carbon black (CB)	**930-5-O_2 (2.1 µm)**	38.5	0.7	2.3	1.6	0.8	1.1
	900-5-O_2 (810 nm)	38.9	0.7	0.4	0.8	0.9	4.3
	810-5-O_2 (240 nm)	34.5	4.3	4.5	3.7	4.0	4.1
$LiF/Li_xPF_yO_z$	**930-5-O_2 (2.1 µm)**	2.6	27.6	39.4	21.9	40.9	29.4
	900-5-O_2 (810 nm)	2.9	25.0	26.0	24.9	47.4	39.4
	810-5-O_2 (240 nm)	2.3	23.3	18.9	20.4	31.1	20.9
Carbonaceous species	**930-5-O_2 (2.1 µm)**	23.3	68.3	51.4	70.9	54.1	65.8
	900-5-O_2 (810 nm)	23.3	71.5	71.5	68.0	48.2	52.2
	810-5-O_2 (240 nm)	25.3	66.4	72.2	72.4	62.5	71.3

AUTHOR INFORMATION

Corresponding author

* Laurence Croguennec

Laurence.Croguennec@icmcb.cnrs.fr

* Delphine Flahaut

delphine.flahaut@univ-pau.fr